opposing effects, it seems reasonable to estimate the overall systematic errors in force at ≤~30%.

23. B. Krummel and M. J. Chamberlin, *J. Mol. Biol.* **225**, 239 (1995); E. Nudler, A. Goldfarb, M. Kashlev, *Science* **265**, 793 (1994); D. Wang *et al.*, *Cell* **81**, 341 (1995); E. Nudler, M. Kashlev, V. Nikiforov, A. Goldfarb, *ibid.*, p. 351.
24. H. Yin *et al.*, data not shown.
25. This estimate is a lower limit because it includes data from complexes that did not stall before reaching the trap limit and because we cannot exclude the possibility that some events classified as stalls may in fact be lengthy transcriptional pauses (*16*).
26. S. M. Block, *Trends Cell Biol.* **5**, 169 (1995).
27. J. T. Finer, R. M. Simmons, J. A. Spudich, *Nature* **368**, 113 (1994); J. T. Finer, A. D. Mehta, J. A. Spudich, *Biophys. J.* **68**, 291s (1995); A. Ishijima *et al.*, *Biochem. Biophys. Res. Commun.* **199**, 1057 (1994); H. Miyata *et al.*, *Biophys. J.* **68**, 286s (1995).
28. A. J. Hunt, F. Gittes, J. Howard, *Biophys. J.* **67**, 766 (1994).
29. Underestimation of F_{stall} (*25*) will cause underestimation of the maximum energy conversion efficiency. Moreover, our efficiency calculation assumes that stalling occurs when the free energy available to drive movement in one cycle of the chemical reaction balances the free energy required to translocate 1 bp along the DNA against the applied force. However, stalling could also occur because of structural alterations in the transcription complex (for example, stabilization of a catalytically inactive enzyme conformation by the applied force). In that case, the maximum efficiency calculated from F_{stall} would underestimate the true efficiency. In contrast, enzymatic consumption of NTPs uncoupled to translocation would reduce the energy conversion efficiency below that calculated from F_{stall}. Although little such consumption has been reported for transcription complexes in solution [for example, see M. Chamberlin, R. L. Baldwin, P. Berg, *J. Mol. Biol.* **7**, 334 (1963)], we cannot exclude the possibility that such uncoupled reactions are catalyzed by immobilized enzyme molecules subjected to the high applied forces used in the stalling experiments. Estimates of energy conversion efficiency from the stall forces of single kinesin and myosin molecules carry analogous uncertainties. Recent evidence (*11*) suggests that kinesin is not tightly coupled near stall.
30. *Escherichia coli* plasmids that carry multiple transcription units can accumulate high densities of transcription-induced supercoils (*31*). This effect can be observed in the absence of DNA gyrase or topoisomerase I activities (which relax negative or positive supercoils, respectively) when one or more of the transcribed genes encodes a membrane-interacting protein (*5*). Specific linking differences (σ) of −0.013 in topoisomerase I mutants [D. N. Cook, D. Ma, N. G. Pon, J. E. Hearst, *Proc. Natl. Acad. Sci. U.S.A.* **89**, 10603 (1992)] and 0.024 in the presence of a DNA gyrase inhibitor [H. Y. Wu, S. H. Shyy, J. C. Wang, L. F. Liu, *Cell* **53**, 433 (1988)] have been reported. RNA polymerase transcription is accompanied by an obligatory rotation relative to the DNA helix. Therefore, the supercoiling torque τ_s [($|\sigma|$) 1.4×10^{-19} N m rad^{-1} (*31*)] is expected to exert a force opposing translocation that is estimated by $F_s = 2\pi\tau_s/h$, where h is the pitch of the DNA helix, 3.6 nm. F_s = 3 and 6 pN, respectively, in the two cited cases. However, this calculation may underestimate the force by a factor of ~2 because supercoils in vivo are thought to be confined to a limited portion of the plasmid DNA.
31. L. F. Liu and J. C. Wang, *Proc. Natl. Acad. Sci. U.S.A.* **84**, 7024 (1987).
32. Supported by grants from the National Institute of General Medical Sciences to J.G., R.L., and S.M.B. M.D.W. was supported by a Damon Runyon–Walter Winchell Cancer Research Fund postdoctoral fellowship. K.S. and S.M.B. thank the Rowland Institute for Science for support during the early stages of this work. A movie of the experiment shown in Fig. 2A can be viewed on the World Wide Web at http://www.rose.brandeis.edu/users/gelles/stall/.

11 August 1995; accepted 26 October 1995

Minimization of a Polypeptide Hormone

Bing Li, Jeff Y. K. Tom, David Oare, Randy Yen, Wayne J. Fairbrother, James A. Wells,* Brian C. Cunningham*

A stepwise approach for reducing the size of a polypeptide hormone, atrial natriuretic peptide (ANP), from 28 residues to 15 while retaining high biopotency is described. Systematic structural and functional analysis identified a discontinuous functional epitope for receptor binding and activation, most of which was placed onto a smaller ring (Cys^6 to Cys^{17}) that was created by repositioning the ANP native disulfide bond (Cys^7 to Cys^{23}). High affinity was subsequently restored by optimizing the remaining noncritical residues by means of phage display. Residues that flanked the mini-ring structure were then deleted in stages, and affinity losses were rectified by additional phage-sorting experiments. Thus, structural and functional data on hormones, coupled with phage display methods, can be used to shrink the hormones to moieties more amenable to small-molecule design.

The generation of leads for drug design is usually achieved through a laborious discovery process wherein a large number of small molecules are screened for binding to a particular receptor or for modulation of a particular biological response. Although structure-based approaches have been used in some cases for generating candidate molecules directly (*1*), this approach has been limited to binding sites for small substrate molecules or short, continuous peptide segments.

Protein-protein interactions are crucial events in most biological processes and are therefore important targets for drug design. Such interfaces are generally large (600 to more than 1300 Å^2), with 10 to 30 contact side chains on each side of the interface (*2*). Moreover, each patch of contact residues is presented from peptide segments that are often distant in primary sequence. Mimicking such large and discontinuous binding surfaces with rationally designed small molecules is a daunting prospect, but it may be simplified because only a small subset of contact side chains appears to be necessary for tight binding at these interfaces (*3*). Displaying these functional epitopes on minimal structured scaffolds may permit smaller candidate compounds to be generated that bind at protein-protein interfaces.

Atrial natriuretic peptide is a 28-residue peptide hormone that is important for regulation of blood pressure and salt balance (*4*). Smaller ANP peptides produced by the screening of synthetic analogs are at least 500 times weaker in receptor-binding affinity (*5*). It is likely that the binding of ANP to its signaling receptor is highly sensitive to the conformation of ANP, as indicated by the loss of binding caused by the reduction of its single disulfide bond. Using a constrained scaffold designed to preserve the structural presentation of the critical binding determinants, we present a systematic strategy for reducing the size of ANP while maintaining high binding affinity and biopotency.

The first step in our minimization process (Fig. 1) was to determine which ANP residues are important for binding to the extracellular domain of the natriuretic peptide receptor–A (NPR-A) by alanine-scanning mutagenesis (*6*). Each of the 28 residues in ANP was converted to alanine, except those comprising the Cys^7 to Cys^{23} disulfide and Ala^{17}. An enzyme-linked immunosorbent assay (ELISA) of these ANP mutants, produced as peptide fusions with gene III coat protein on phage (*7*), allowed us to rapidly assess the relative binding affinity of the mutants by eliminating the need to purify each peptide to homogeneity. Mutations at only seven positions (Phe^8, Met^{12}, Asp^{13}, Arg^{14}, Ile^{15}, Leu^{21}, and Arg^{27}) each resulted in an affinity that was more than 10 times lower than that of wild-type ANP (Fig. 2). These results are consistent with effects on an aortic ring contraction assay reported for substitutions with D-amino acids or alanines in ANP (*8*).

Five of the seven most important residues (Phe^8, Met^{12}, Asp^{13}, Arg^{14}, and Ile^{15}) formed a small functional epitope on one side of the hormone (Fig. 3A). On the basis of the structure of ANP (*9*), three alternative disulfide forms of the molecule (Cys^7 to Cys^{17}, Cys^6 to Cys^{17}, and Cys^5 to Cys^{17}) were designed to isolate this functional epitope on a smaller disulfide ring and eliminate the native Cys^7 to Cys^{23} disulfide (Fig. 3B). Of these three variants, Cys^6 to Cys^{17} was the best, albeit with an affinity that was more than 100 times lower than

B. Li, W. J. Fairbrother, J. A. Wells, B. C. Cunningham, Department of Protein Engineering, Genentech, 460 Point San Bruno Boulevard, South San Francisco, CA 94080, USA.
J. Y. K. Tom and D. Oare, Bioorganic Chemistry, Genentech, 460 Point San Bruno Boulevard, South San Francisco, CA 94080, USA.
R. Yen, Medicinal and Analytical Chemistry, Genentech, 460 Point San Bruno Boulevard, South San Francisco, CA 94080, USA.

*To whom correspondence should be addressed.

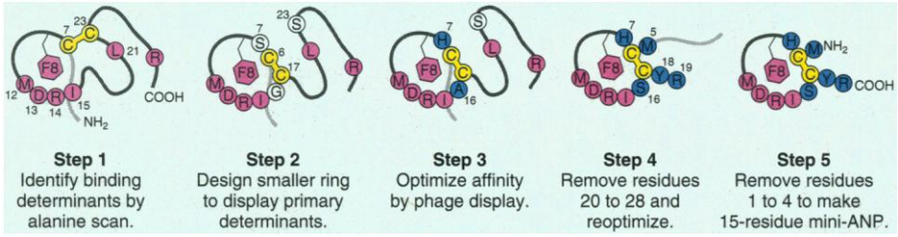

Fig. 1. Strategy used to shrink ANP (28 aa) to mini-ANP (15 aa). **Step 1**: Alanine-scanning mutagenesis of ANP displayed on phage identified seven residues (highlighted in magenta) that were most important for binding to the NPR-A receptor; five of these residues form a tight cluster (Fig. 2). **Step 2**: Based on the structure of ANP (Fig. 3), an alternate Cys^6-Cys^{17} disulfide cross-link (yellow) was designed that reduced binding affinity to a value 100 times lower than that of the wild-type ANP. **Step 3**: Binding affinity was restored by randomly mutating noncritical residues and selecting mutations by phage display that improved affinity (highlighted in blue). **Step 4**: COOH-terminal residues were deleted and the peptide was reoptimized by phage display to yield a 19-aa peptide whose affinity for NPR-A was about 20 times less (weaker) than that of wild-type ANP. **Step 5**: The four NH_2-terminal residues were deleted to yield a 15-aa peptide whose affinity for NPR-A was about five times weaker than that of wild-type ANP.

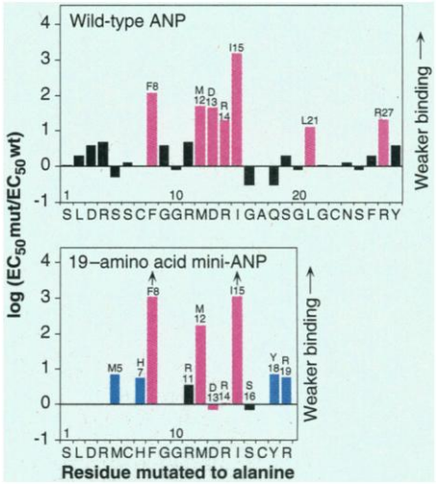

Fig. 2. Functional importance of side chains in wild-type ANP (upper panel) or the optimized 19-aa peptide (lower panel) as assessed by alanine-scanning mutagenesis of the peptides displayed on phage. Binding to the NPR-A receptor was assayed by phage ELISA (*7*) and used to calculate relative affinities expressed as $\log(EC_{50}$ mutant/EC_{50} wild type) on the *y* axis. Thus, numbers above zero indicate the reduction in affinity that occurs after side chain atoms beyond the β-carbon (for nonglycine substitutions) are removed by alanine substitution of the wild-type residue shown on the *x* axis. Alanine substitutions in wild-type ANP or the optimized 19-aa peptide, which cause at least 10 times lower affinities, are shown in magenta. Residues that were fixed by phage selection in the optimized 19-aa peptide are shown in blue. Alanine substitutions of Phe^8 and Ile^{15} in the 19-aa peptide result in greater than 1000 times lower affinites (indicated by arrows in lower panel).

Table 1. Relative affinities for the NPR-A receptor of selected ANP variants that were fused to phage or assayed as free peptides (*18*). The affinity for wild-type ANP on phage or as a free peptide was 500 pM and 50 pM, respectively. Numbers in each column indicate the relative reductions in binding compared to wild-type ANP, calculated as EC_{50} mutant/EC_{50} wild type. Phage displaying variants 1 to 5 used a Glu-Gly-Gly spacer fused to gene III at residue + 198; phage displaying variants 6 to 7 used a Gly-Gly-Gly spacer fused at residue +198; phage displaying variants 8 and 9 used a longer $(Gly\text{-}Gly\text{-}Gly\text{-}Ser)_2$ spacer fused to gene III at residue +317 (Table 2). Numerical subscripts indicate the position of the preceding cysteines relative to Phe or Cha (cyclohexylalanine) at position 8. Phage affinities were determined by phage ELISA and peptide affinities were measured by RIA (*7*). ND, not determined.

ANP variant	Relative phage affinity for NPR-A	Relative peptide affinity for NPR-A
1 $SLRRSSC_7FGGRMDRIGAQSGLGC_{23}NSFRY$	1	1
2 $SLRRSSC_7FGGRMDRIGC_{17}QSGLGSNSFRY$	>1,500	ND
3 $SLRRSC_6SFGGRMDRIGC_{17}QSGLGSNSFRY$	104	ND
4 $SLRRC_5SSFGGRMDRIGC_{17}QSGLGSNSFRY$	480	ND
5 $SLRRSC_6HFGGRMDRIAC_{17}QSGLGSNSFRY$	1	ND
6 $SLRRSC_6HFGGRMDRIAC_{17}$	300	40,000
7 $SLRRSC_6HFGGRMDRIAC_{17}$NR-short spacer	8	43
8 $SLRRSC_6HFGGRMDRIAC_{17}$NR-long spacer	50	43
9 $SLRRMC_6HFGGRMDRISC_{17}$YR-long spacer	8	6
10 $MC_6HFGGRMDRISC_{17}YR$	ND	7
11 RC_7(Cha)$GGRIDRIFRC_{18}$	ND	7,200

that of wild-type ANP (Table 1, variants 2 to 4). Despite this large reduction in binding, the Cys^6 to Cys^{17} variant binds NPR-A more tightly than reported for the Cys^7 to Cys^{18} or linear ANP forms (*10*, *11*).

Monovalent phage display (*12*) was applied to improve the affinity of the Cys^6 to Cys^{17} ANP variant (Fig. 1, step 3). Noncritical residues (Ser^7, Gly^9, Gly^{10}, Arg^{11}, and Gly^{16}) within the Cys^6 to Cys^{17} disulfide loop were mutated simultaneously to all 20 possibilities (Table 2, library 1). After six rounds of selecting phage for binding NPR-A immobilized on plates, virtually every phage selected contained S7H and G16A (*13*), whereas the wild-type residues Gly^9, Gly^{10}, and Arg^{11} were retained (*14*). This mutant had nearly the same affinity as wild-type ANP and therefore was 100 times improved compared with the starting Cys^6 to Cys^{17} mutant (Table 1, variant 5).

We next shortened the COOH-terminal portion of the molecule by deleting residues Gln^{18} through Tyr^{28} (Fig. 1, step 4). This reduced the affinity by 300 times presumably as a result of the loss of some binding determinants (Leu^{21} and Arg^{27}) and a possible distortion of the primary binding epitope (Table 1, variant 6). To recover binding affinity, we sorted three new phage display libraries (Table 2, libraries 2 to 4). These contained two, three, or four randomized residues after Cys^{17}. Most of the phage selected from these libraries incorporated Q18N and S19R.

The 19–amino acid (aa) peptide containing the Q18N and S19R substitutions bound to NPR-A with an affinity that was only eight times weaker than that of the wild-type ANP when displayed on phage (Table 1, variant 7). This peptide was synthesized, and the binding affinity to NPR-A was determined to be 43 times weaker than that of the wild-type ANP. We also synthesized the prototype 17-aa peptide (Table 1, variant 6); instead of its binding being 300 times weaker than that of wild type (as expected from the phage ELISA), it was 40,000 times weaker. We hypothesized that this discrepancy (a factor of 5 to 100) between the binding of peptides fused to phage compared with the free peptide could result if the sequence of the gene III protein near the cyclic peptide contributed fortuitous binding determinants. To test this, we placed a longer spacer sequence $(Gly\text{-}Gly\text{-}Gly\text{-}Ser)_2$ after residue 19 and fused it to a different place in the gene III protein (beginning at position 317). Indeed, the binding of this analog was 50 times weaker than that of the wild-type ANP, a value consistent with the 43 times lower binding measured for the synthetic peptide (Table 1, variant 8).

The 19-aa peptide was then reoptimized on phage with the use of the longer spacer, by randomizing the four residues immediately flanking the Cys^6 to Cys^{17} disulfide bond (Table 2, library 5). The selectant with highest affinity introduced S5M, A16S, and $N18Y$ and retained His^7. On phage this variant bound only eight times weaker than wild-type ANP and as an isolated peptide only six times weaker (Table 1, variant 9).

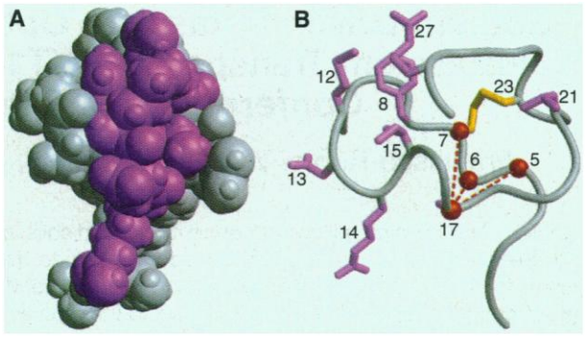

Fig. 3. Structural models of ANP used to design smaller versions of the hormone. (**A**) Space-filling model showing the clustering of NPR-A receptor-binding determinants identified by alanine scanning (Fig. 2). The binding determinants Phe[8], Met[12], Asp[13], Arg[14], Ile[15], Leu[21], and Arg[27] (highlighted in magenta) account for most of the hormone's receptor-binding affinity. The model was derived from nuclear magnetic resonance structural coordinates of an ANP variant (*20*). (**B**) α-Carbon tracing illustrating three proposed alternate disulfide cross-links (red) that places much of the functional epitope on smaller rings. The ensemble average distances, between the α-carbons at position 17 and the proposed cross-links to positions 5, 6, and 7, for 11 energy-minimized structures, are 6.6 ± 1.2, 7.3 ± 1.2, and 8.8 ± 0.6 Å, respectively. The native 7 to 23 disulfide bond and the seven most dominant binding determinants are shown in yellow and magenta, respectively. The image in (B) is rotated left 90° about its vertical axis relative to the image in (A).

Table 2. Phage libraries displaying randomized ANP molecules. Residues designated as *X* were randomized to all 20 natural amino acids as described (*19*). Each library consisted of 4×10^7 to 22×10^7 independent transformants and theoretically covered all possible sequence combinations. The randomized ANP molecules were fused via a glycine-rich spacer to the COOH-terminal gene III segment as shown below.

Positions randomized	Spacer	Position of gene III fusion
1 SLDRSC$_6$XFXXX-MDRIXC$_{17}$QSGL-GSNSFRY	EGG	+198
2 SLDRSC$_6$HFG-GRMDRIAC$_{17}$XX	GGG	+198
3 SLDRSC$_6$HFGG-RMDRIAC$_{17}$XXX	GGG	+198
4 SLDRSC$_6$HFG-GRMDRIAC$_{17}$XXXX	GGG	+198
5 SLDRXC$_6$XFGG-RMDRIXC$_{17}$XR	(GGGS)$_2$	+317

We analyzed the functional importance of the selected and conserved residues in the optimized 19-aa peptide by alanine scanning and phage ELISA (Fig. 2B). The most important determinants were the hydrophobic side chains Phe[8], Met[12], and Ile[15], which decreased the affinity 100 to 1000 times when converted to alanine. These were also the most dominant determinants in the full-length ANP (Fig. 2A), suggesting that the basic structural and functional epitopes were similar whether presented from the wild-type scaffold or the shortened peptide. These residues appear to be more important in the context of the smaller scaffold, indicating that the functional epitope may be more concentrated. However, three of the important residues in the wild-type hormone (Asp[13], Arg[14], and Leu[21]) were no longer important in the selected 19-aa peptide. Perhaps their roles had been replaced by the newly selected residues, Met[5], His[7], Tyr[18], and Arg[19]. Indeed, when

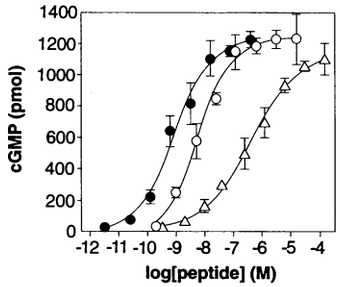

Fig. 4. Potency of mini-ANP peptides for stimulating cGMP production in 293 cells transiently expressing NPR-A (*21*). EC_{50} values calculated from four-parameter curve fits were 0.78 nM for wild-type ANP (●), 5.9 nM for variant 10 (○, mini-ANP), and 430 nM for variant 7 (△). Each data point and error bar represents the mean of three replicates ± SD.

any one of these was converted to alanine, the affinity decreased 8 to 10 times (Fig. 2B). Thus, this minimization process appeared to preserve the dominant features of the functional epitope while recruiting local functional determinants. These changes compensate for the perturbations caused by the deletions and the alternative Cys[6] to Cys[17] disulfide bond.

Finally, we deleted the first four residues on the optimized 19-aa peptide (Fig. 1, step 5) because the alanine scan of the wild-type ANP showed that these residues were only of minor importance. The resulting 15-aa peptide was synthesized and then amidated on its COOH-terminus to better mimic the presentation of the peptide on phage. This peptide, which we call mini-ANP, bound with an affinity that was only seven times lower than that of the wild-type ANP (Table 1, variant 10). We measured the biopotency of several of these peptides (Fig. 4) by their ability to stimulate guanosine 3′5′-monophosphate (cGMP) production in cells that express NPR-A (*14*). The median effective concentration (EC_{50}) for wild-type ANP was 0.8 nM compared with 5.9 nM for the mini-ANP 15-aa peptide (variant 10) and 430 nM for the 19-aa peptide (variant 7). This biopotency corresponds to a 7.6 times lower affinity for the mini-ANP variant relative to wild-type ANP and is consistent with the 7.4 times lower affinity for NPR-A binding measured for this peptide (*15*). Thus, the size of the hormone was reduced nearly 50% while retaining high binding affinity for NPR-A (EC_{50} = 0.48 nM) and biopotency (EC_{50} = 5.9 nM). This can be compared with one of the best reported smaller versions of ANP, a 13-aa peptide derived by more standard medicinal chemistry methods (*11*) with an EC_{50} of 470 nM or 7200 times lower affinity relative to the wild-type ANP (Table 1, variant 11).

Previous studies have shown that it is possible to graft protein-binding determinants between antibodies or structurally homologous hormone scaffolds (*16*). In contrast, attempts to place catalytic groups from a serine protease onto a cyclic peptide without preserving the original structure have failed (*17*). Our structure-based approach to minimization attempts to preserve the functional epitope while maintaining its structure on a smaller scaffold. Phage display was paramount for rectifying the imperfections present in the smaller designs. This method may be generally useful for generating peptide leads for other polypeptide hormones.

REFERENCES AND NOTES

1. M. von Itzstein *et al.*, *Nature* **363**, 418 (1993); B. K. Shoichet, R. M. Stroud, D. V. Santi, I. D. Kuntz, K. M. Perry, *Science* **259**, 1445 (1993); R. S. McDowell *et al.*, *J. Am. Chem. Soc.* **116**, 5069 (1994); E. A. Lunney *et al.*, *J. Med. Chem.* **37**, 2664 (1994); P. Y. Lam *et al.*, *Science* **263**, 380 (1994); M. A. Navia and M. A. Murcko, *Curr. Opin. Struct. Biol.* **2**, 202 (1992).
2. J. Janin and C. Chothia, *J. Biol. Chem.* **265**, 16027 (1990); A. M. de Vos, M. Ultsch, A. A. Kossiakoff, *Science* **255**, 306 (1992); D. R. Davies, E. A. Padlan, S. Sheriff, *Annu. Rev. Biochem.* **59**, 439 (1990).
3. B. C. Cunningham and J. Wells, *J. Mol. Biol.* **234**, 554 (1993); T. Clackson and J. A. Wells, *Science* **267**, 383 (1995); R. F. Kelley and M. P. O'Connell, *Biochemistry* **32**, 6828 (1993); L. Jin, B. M. Fendly, J. A. Wells, *J. Mol. Biol.* **226**, 851 (1992); J. M. Nuss, P. B. Whitaker, G. M. Air, *Proteins* **15**, 121 (1993); W. R. Tulip, V. R. Harley, R. G. Webster, J. Novotny, *Biochemistry* **33**, 7986 (1994).
4. T. Maack, *Annu. Rev. Physiol.* **54**, 11 (1992).
5. R. M. Scarborough *et al.*, *J. Biol. Chem.* **261**, 12960 (1986); see P. R. Bovy *et al.* (*10*); T. W. von Geldern *et al.*, *J. Med. Chem.* **35**, 808 (1992).
6. B. C. Cunningham and J. A. Wells, *Science* **244**, 1081 (1989); J. A. Wells, *Methods Enzymol.* **202** (1991).
7. B. C. Cunningham, D. G. Lowe, B. Li, B. D. Bennett, J. A. Wells, *EMBO J.* **13**, 2508 (1994). A phage ELISA was used to quantitate the binding affinity of ANP displaying phage to NPR-A. Alanine mutants of ANP were displayed on the pB1537 phagemid that contained two additional mutations (R3D in ANP and Q29E in the spacer residue immediately after residue 28 of ANP) that increase the efficiency of ANP display without affecting NPR-A–binding affinity (B. Li *et al.*, unpublished data). For Fig. 2 (upper panel) affinities were based on phage ELISA measurements, except those for F8A and I15A, which were determined from radioimmunoassay (RIA) measurements of the respective peptides.
8. R. F. Nutt *et al.*, in *Synthetic Peptides: Approaches to*

Biological Problems, J. P. Tam and E. T. Kaiser, Eds. (Liss, New York, 1989), pp. 267–279; R. F. Nutt *et al.*, in *Peptides: Chemistry, Structure and Biology*, J. E. Rivier and G. R. Marshall, Eds. (ESCOM, Leiden, Netherlands, 1988), pp. 444–446.
9. W. J. Fairbrother, R. S. McDowell, B. C. Cunningham, *Biochemistry* **33**, 8897 (1994).
10. P. R. Bovy *et al.*, *J. Biol. Chem.* **264**, 20309 (1989).
11. T. W. von Geldern *et al.*, *J. Med. Chem.* **35**, 808 (1992).
12. S. H. Bass, R. Greene, J. A. Wells, *Proteins Struct. Funct. Genet.* **8**, 309 (1990); H. B. Lowman and J. A. Wells, *J. Mol. Biol.* **234**, 564 (1993); J. A. Wells and H. B. Lowman, *Curr. Opin. Struct. Biol.* **2**, 597 (1992).
13. Single-letter abbreviations for the amino acid residues are as follows: A, Ala; C, Cys; D, Asp; E, Glu; F, Phe; G, Gly; H, His; I, Ile; K, Lys; L, Leu; M, Met; N, Asn; P, Pro; Q, Gln; R, Arg; S, Ser; T, Thr; V, Val; W, Trp; and Y, Tyr. Mutations are designated by the wild-type residue, followed by its position and the mutant residue. Multiple mutations are indicated by a series of single mutations separated by hyphens.
14. B. Li and B. C. Cunningham, unpublished data.
15. The decrease (550 times lower) in bioactivity measured for the original 19-aa peptide compared with its 43 times lower receptor affinity may reflect a number of factors, including the susceptibility of this peptide to proteolysis in cell culture or kinetic parameters involved in receptor activation.
16. P. T. Jones, P .H. Dear, J. Foote, M. S. Neuberger, G. Winter, *Nature* **321**, 522 (1986); B. C. Cunningham, D. J. Henner, J. A. Wells, *Science* **247**, 1461 (1990); L. Presta, *Annu. Rep. Med. Chem.* **29**, 317 (1994).
17. J. A. Wells, W. J. Fairbrother, J. Otlewski, M. Laskowski, J. Burnier, *Proc. Natl. Acad. Sci. U.S.A.* **91**, 4110 (1994); D. R. Corey and M. A. Phillips, *ibid.*, p. 4106.
18. Peptides were synthesized on an Applied Biosystems 430A automated synthesizer according to standard *N-tert*-butoxycarbonyl chemistry protocols, cleaved off the resin with anhydrous HF at 0°C, then cyclized by the potassium ferricyanide method and purified by reversed-phase high-performance liquid chromatography. Masses of each peptide were verified by mass spectrometry. All the peptides except for variant 6 were synthesized with an amidated COOH-terminus.
19. Phagemid libraries that displayed variants of ANP contained codons that were randomized to all 20 amino acids by site-directed mutagenesis [T. A. Kunkel, J. D. Roberts, R. A. Zakour, *Methods Enzymol.* **154**, 367 (1987)] with the following oligonucleotides that changed target codons to NNS sequences (N is a mixture of all four bases and S is a mixture of G and C bases): 5′-TCTCTGGATAGATCTTGC(NNS)TTC(NNS)$_3$ATGGATCGTATC(NNS)TGCCAGAGCGGT-3′ for library 1, 5′-ATGGATCGTATCGCGTGC(NNS)$_2$-GGGGGCGGCC-C-3′ for library 2, 5′-ATGGATCGTATCGCGTGC-(NNS)$_3$-GGGGGCGGG-CCC-3′ for library 3, 5′-ATGGATCGTATCGCTGC(NNS)$_4$-GGGG-GCGGGCCC-3′ for library 4, and 5′-TATGCATCTCTGGATAGA-(NNS)TGC(NNS)TTCGGGGGCCGGATGGATCGTATC(NNS)TGC(NNS)CGGGGGGGCGGGTCT-3′ for library 5. Each library consisted of 4×10^7 to 22×10^7 independent mutants and theoretically represented all possible sequence combinations. To minimize wild-type background, the mutagenesis template used for libraries 2 to 5 was frameshifted within the region to be randomized.
20. The molecular models (Fig. 3) are from 1 of 11 energy-minimized structures of an ANP variant (*9*) whose coordinates are deposited in the Brookhaven Protein Data Bank (accession number 1ANP). This model of wild-type ANP contains two substitutions (L12M-S14R), which revert back mutations that were present in the variant whose structure was solved.
21. B. C. Cunningham, D. G. Lowe, B. Li, B. D. Bennett, J. A. Wells, *EMBO J.* **13**, 2508 (1994); B. D. Bennett *et al.*, *J. Biol. Chem.* **266**, 23060 (1991).
22. We thank D. Lowe for providing the immunoglobulin G–receptor fusion protein and for advice; B. McDowell for discussions; the DNA synthesis group for oligonucleotides; A. Padua for amino acid analysis; and D. Woods, K. Andow, and W. Anstine for help with graphics.

19 June 1995; accepted 18 October 1995

Sodium-Driven Potassium Uptake by the Plant Potassium Transporter HKT1 and Mutations Conferring Salt Tolerance

Francisco Rubio, Walter Gassmann, Julian I. Schroeder

Sodium (Na^+) at high millimolar concentrations in soils is toxic to most higher plants and severely reduces agricultural production worldwide. However, the molecular mechanisms for plant Na^+ uptake remain unknown. Here, the wheat root high-affinity potassium (K^+) uptake transporter HKT1 was shown to function as a high-affinity K^+-Na^+ cotransporter. High-affinity K^+ uptake was activated by micromolar Na^+ concentrations; moreover, high-affinity Na^+ uptake was activated by K^+ (half-activation constant, 2.8 μM K^+). However, at physiologically detrimental concentrations of Na^+, K^+ accumulation mediated by HKT1 was blocked and low-affinity Na^+ uptake occurred (Michaelis constant, ~16 mM Na^+), which correlated to Na^+ toxicity in plants. Point mutations in the sixth putative transmembrane domain of HKT1 that increase Na^+ tolerance were isolated with the use of yeast as a screening system. Na^+ uptake and Na^+ inhibition of K^+ accumulation indicate a possible role for HKT1 in physiological Na^+ toxicity in plants.

Salinization of irrigated lands is an increasing threat to agriculture. Na^+ concentrations [Na^+] of ≥25 mM are frequently found in saline soils, and most crop plants are glycophytes that are sensitive to high [Na^+] (*1*, *2*). Physiological studies indicate that Na^+ tolerance in plants is determined by several components (*1*, *2*), including osmolyte synthesis (*3*), Na^+ sensitivity of vital enzymes (*4*), and ion transport processes (*5–9*). It has been suggested that reducing Na^+ accumulation is crucial for engineering Na^+ tolerance in plants (*8*, *10*). However, the molecular mechanisms for Na^+ uptake and exclusion in plants remain unknown.

Recently, a complementary DNA (cDNA) from wheat, *HKT1*, was isolated that encodes a high-affinity K^+ uptake transporter (*11*), and in roots of *Arabidopsis thaliana*, voltage-clamp recordings of high-affinity K^+ uptake were reported (*12*). Current-voltage studies of the mechanism of K^+ uptake through HKT1 showed a variation in HKT1-mediated currents, which indicated that additional relevant transported factors remained unknown (*11*). Initial experiments showed that HKT1-mediated currents are affected by Na^+ (*11*). Here, we show that HKT1 mediates high-affinity K^+-Na^+ cotransport and low-affinity Na^+ uptake in a manner consistent with Na^+ toxicity in plants, and we identify mutations that improve HKT1-mediated Na^+ tolerance.

In control tracer flux experiments (*13*) with untransformed K^+ uptake–deficient yeast strains (*14*), neither $^{86}Rb^+$ (K^+) nor $^{22}Na^+$ uptake was observed (Fig. 1, filled symbols). In HKT1-expressing yeast cells, Na^+ strongly stimulated Rb^+ uptake (half-activation constant $K_{1/2}$ = 175 ± 50 μM Na^+, mean ± SD; n = 4) (Fig. 1A). $^{22}Na^+$ flux experiments in yeast allowed us to determine whether Na^+ uptake was mediated by HKT1 or whether Na^+ was merely enhancing Rb^+ accumulation (*15*). $^{22}Na^+$ uptake experiments in HKT1-expressing yeast demonstrat-

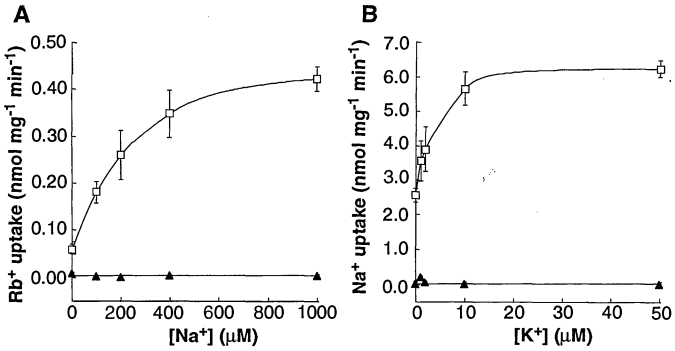

Fig. 1. HKT1 expressed in yeast gives rise to Na^+-stimulated Rb^+ uptake (**A**) and to K^+-stimulated Na^+ uptake (**B**) [□, yeast cells expressing HKT1; ▲, K^+ uptake–deficient yeast mutants (*14*)]. In (A), the initial rate of Rb^+ uptake is represented as a function of increasing external Na^+. In (B), the initial rate of Na^+ uptake is represented as a function of increasing external K^+. Uptake experiments were carried out at pH 6.0, 30°C, in the presence of 15 μM Rb^+ (A) or 200 μM Na^+ (B) (*13*). At nominally 0 [Na^+], a Rb^+ uptake rate of 0.05 nmol mg^{-1} min^{-1} was observed (A), and at nominally 0 [K^+], a Na^+ uptake rate of 2.6 nmol mg^{-1} min^{-1} was observed (B). This can likely be attributed to the background [Na^+] (11 μM) and [K^+] (2 μM) in the buffer used for the uptake experiments, as determined by atomic absorption spectrophotometry.